Analysis and Design of a Control Strategy for Tracking Sinusoidal References in Single-Phase Grid-Connected Current-Source Inverters

Carlos R. Baier, *Member, IEEE*, Miguel A. Torres, *Member, IEEE*, Pablo Acuna, *Member, IEEE*, Javier A. Muñoz, *Member, IEEE*, Pedro E. Melín, *Member, IEEE*, Carlos Restrepo, and Johan I. Guzman, *Member, IEEE*

***Abstract*—A novel control strategy for single-phase current-source inverters connected to an ac grid is proposed in this paper. The control strategy aims to inject maximum power to the grid under transient and steady-state conditions by the tracking of sinusoidal references. This paper presents the modeling and the design of the control strategy based on the exact linearization of the inverter model. Results are obtained by computational simulation and validated experimentally. By using error performance indexes in the analysis of the results, it is demonstrated that the proposed controllers achieve correct tracking of the sinusoidal reference while keeping a low switching frequency, which helps to minimize the commutation losses.**

***Index Terms*—Current-source inverter (CSI), dc–ac power conversion, grid-connected inverters, nonlinear control strategies.**

I. Introduction

NOWADAYS, single-phase inverters are widely used in residential renewable energy systems due to the single-phase nature of residential electrical grids. However, it is also possible to find single-phase inverters in three-phase industrial applications, for example, in the form of the so-called power cells in modular or multicell topologies [1]. Although single-phase inverters can be found in different applications, recent advances and development efforts have been concentrated in distributed generation systems involving transformer-less inverters for bidirectional power injection into ac grids [2].

Manuscript received August 5, 2016; revised November 12, 2017 and January 4, 2017; accepted February 3, 2017. Date of publication February 13, 2017; date of current version October 6, 2017. This work was supported by the Chilean Government under Project CONICYT/FONDECYT 1160969 and Project CONICYT/FONDECYT 11150069. Recommended for publication by Associate Editor G. Oriti.

C. R. Baier, J. A. Muñoz, C. Restrepo, and J. I. Guzman are with the Department of Electrical Engineering, Universidad de Talca, Curicó 747-C, Chile (e-mail: cbaier@utalca.cl; jamunoz@utalca.cl; crestrepo@utalca.cl; jguzmand@utalca.cl).

M. A. Torres is with the Institute of Engineering Sciences, Universidad de O'Higgins, Rancagua 2820000, Chile (e-mail: miguel.torres@uoh.cl).

P. Acuna is with the School of Electrical Engineering and Telecommunications, University of New South Wales, Sydney, NSW 2052, Australia (e-mail: pablo.acuna@unsw.edu.au).

P. E. Melín is with the Department of Electrical and Electronic Engineering, Universidad del Bío-Bío, Concepción, 5-C, Chile (e-mail: pemelin@ubiobio.cl).

Color versions of one or more of the figures in this paper are available online at http://ieeexplore.ieee.org.

Digital Object Identifier 10.1109/TPEL.2017.2668379

In order to inject power into an ac grid, it is possible to use different single-phase inverter topologies, for instance, the voltage source (VSI) [3]–[6], the quasi-impedance and/or impedance source [7]–[10], and the current source (CSI) [11]–[14]. Several control schemes that aim to manage the injection or absorption of energy from the ac grid have been proposed in the literature to correctly operate these topologies. However, most of the proposed strategies are for voltage-source converters and, therefore, do not give much importance to efficiency into their operation.

In the case of CSIs, both control and efficiency are important issues. The single-phase CSI (SP-CSI) is a topology that has been less explored—than the voltage-source topology—for its use in applications that require supplying single-phase loads or power injection into the ac grids [11], [15], [16]. When compared to other—most popular—topologies, one of the biggest disadvantages of CSIs is their greater conduction losses due to the high levels of current they manage [17], [18]. In this regard, the emergence of new wide-bandgap semiconductors and its promise to considerably reduce conduction losses [19], [20] makes to reconsider the use of CSIs as an attractive power conversion topology.

As mentioned above, for CSIs to appear as a competitive alternative, conduction losses have to be reduced, but switching losses too. However, most of the well-known control strategies that are widely used in power electronics entail high and/or variable commutation frequencies that increase the losses considerably, e.g., sliding mode control based techniques [21], finite-states model-based predictive control, and space vector modulation that consider low modulation indexes [22]–[25]. Therefore, to achieve further improvements in the efficiency of CSIs, it is necessary to count with control strategies that achieve zero error in steady state while maintaining low switching frequencies [25], [26].

For single-phase inverters, there are two known and proved strategies that allow to propose control schemes that can operate with low switching frequencies and at the same time to achieve zero steady-state error; 1) PI control strategies based on synchronous *DQ* reference frame [27], and 2) sinusoidal tracking strategies based on different PWM control methods [24], [27], [28]. Control strategies based on single-phase synchronous DQ reference frame allow to define the single-phase ac variables in

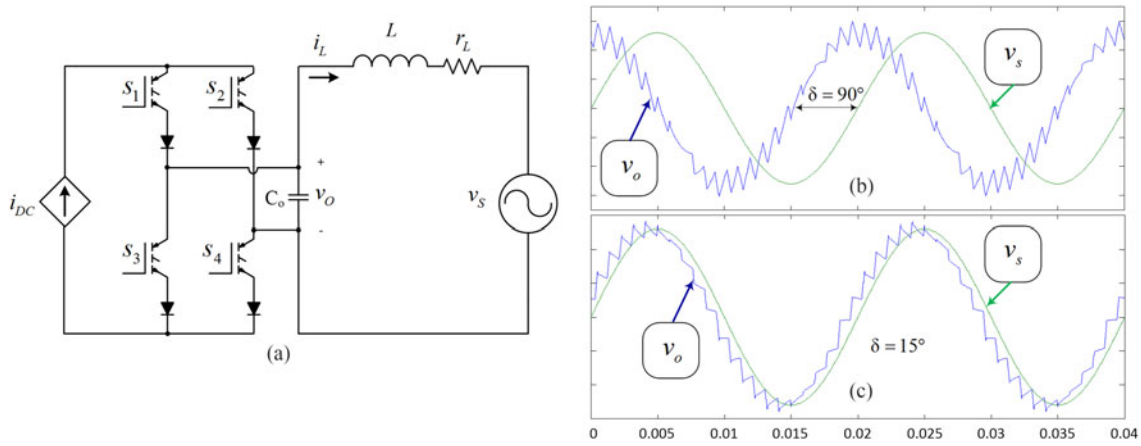

Fig. 1. SP-CSI connected to the grid and associated voltage waveforms: (a) converter topology, (b) inverter output and grid voltage for high level of injected power, and (c) inverter output and grid voltage for low level of injected power.

its *d* and *q* components that reach constant values in steady state, allowing the use of PI controllers. However, to apply the Park transformation to single-phase variables, it is necessary to synthetize an imaginary component for each single-phase variable, which typically is the same variable delayed by 90°. This technique presents two major drawbacks: 1) each *d* and *q* variable will have an inherent delay of 90° due to the delay introduced by the imaginary component in the ac stage, and 2) the resultant control scheme will have the double of the controllers needed to control the ac variables due to their decomposition into *d*- and *q*-axis [14], [27]. On the other hand, sinusoidal tracking strategies directly control the ac variables that need to be controlled, without having to convert them to another domain [24], [27], [28]. For grid-connected single-phase inverters, the dynamics achieved with sinusoidal tracking strategies are much faster than the ones achieved with DQ-based techniques; nevertheless, they typically produce high and/or variable commutation frequencies [24], [29]. Thus, the main challenge when using sinusoidal tracking strategies is to achieve fast dynamic performance while keeping the commutation frequency low [30]–[33]. To design a suitable control strategy that addresses this issue is the major motivation of this paper.

This paper presents a novel control strategy that combines the exact linearization of the SP-CSI and the use of linear controllers for tracking a sinusoidal reference of the inverter output voltage in the ac domain. Two controllers will be analyzed and their performances compared a proportional (P) controller and a proportional-resonant (PR) controller. Both alternatives are simple to implement, achieve low switching frequencies, and fast dynamic response of the single-phase variables, which is especially useful when rapid changes are required in the output power of SP-CSIs. A clear example of the latter application is when CSI are utilized for dynamic frequency control or as grid interfaces in energy storage systems [14], [34].

This paper is organized as follows: Section II gives a brief introduction to the case of CSIs connected to a single-phase ac grid; Section III presents different ways to generate sinusoidal references to inject power from the inverter to a stiff ac grid; Section IV presents control strategies for the output voltage of SP-CSI, which are the result of the exact linearization of the inverter model; Section V includes different simulation results for the SP-CSI controlled by the proposed strategies and Section VI presents the experimental results of a low-power prototype; finally, the conclusions of this work are depicted in Section VII.

II. SP-CSIs Connected to an AC Grid

An SP-CSI can be directly connected to a single-phase grid through a second-order capacitive–inductive filter, as shown in Fig. 1.

Discrete circuit elements designated as L and r_L represent components of the output filter or may also correspond to the equivalent inductance and resistance of the ac line, and v_s is the grid voltage. If nominal output voltage and maximum output power are desired, a phase angle δ—also known as the power angle–between the inverter and grid voltages of 90° is required, as shown in Fig. 1(b). Consequently, in order to inject less power for the same output voltage, the power angle δ should be smaller, as is it shown in Fig. 1(c). In both cases, the output voltage will present a distortion that depends on the size of the output filter capacitor and on the level of injected power, where the higher the power injected by the inverter, the more the distortion its output voltage presents [35].

The output voltage of the SP-CSI shown in Fig. 1(a) can be described with the following equation:

$$\frac{dv_o}{dt} = \frac{1}{C_o}\left(S_{\mathrm{AC}} i_{\mathrm{DC}} - i_L\right) \tag{1}$$

where v_o is the output voltage of the inverter, C_o is the capacitor connected to the inverter's output terminals, S_{AC} corresponds to the switching function of the inverter, i_{DC} is the dc input current to the inverter, and i_L is the output current injected to the ac line.

If the inverter is connected to a stiff grid, as shown in Fig. 1(a), it is possible to write the equation of the connected system as

$$\frac{di_L}{dt} = \frac{1}{L}\left(v_o - r_L i_L - v_s\right) \tag{2}$$

where L is the total line inductance between the inverter and the grid, r_L is the equivalent line resistance and v_s is the voltage imposed by the stiff grid. From (2), it can be noted that by

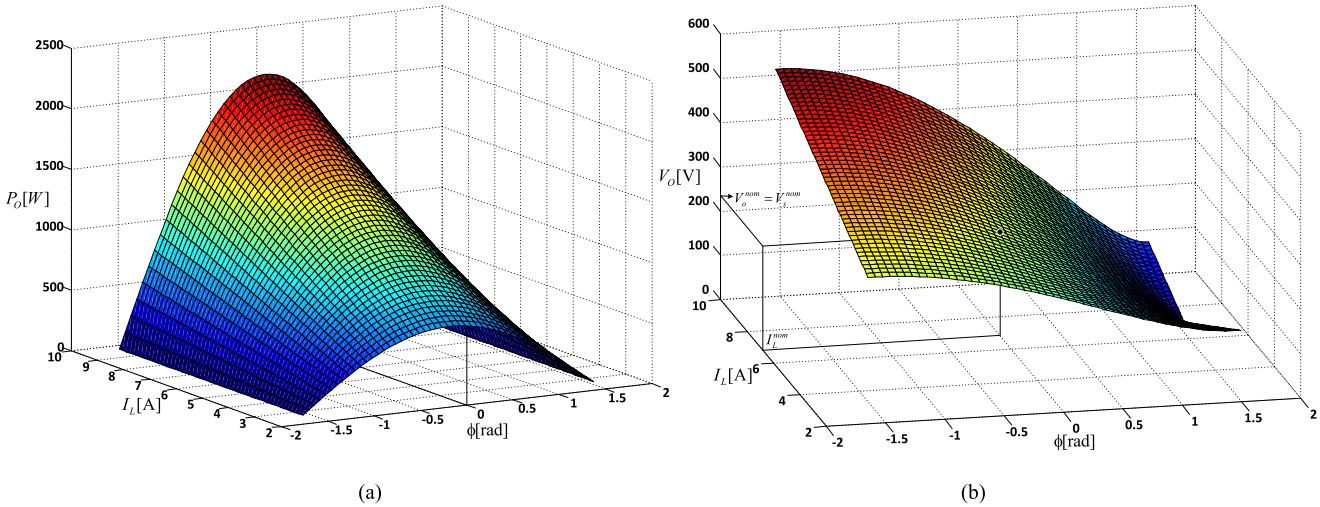

(a) (b)

Fig. 2. Output power and voltage of the SP-CSI as a function of the effective value of output current I_{L} and phase angle ϕ: (a) output power of the SP-CSI and (b) output voltage of the SP-CSI.

controlling the output voltage v_o of the inverter it is possible to modify the effective value of the current i_L. which, in turn, determines the power injected into the grid. The following section explains in detail the use of sinusoidal tracking strategies to control the power injected by the inverter, either by controlling the output voltage or the output current.

III. Sinusoidal References for a Maximum Power Injected From the Single-Phase Inverters

In single-phase grids, there are two manners of controlling the power injected by inverters: 1) by adjusting the magnitude and phase of the current i_L injected by the inverter, and 2) by adjusting the magnitude and phase of the injected voltage with respect to the grid voltage v_o [35]. These two methods will be explained in the following sections. For the analysis, nominal quantities of voltage V_o^{nom}, and current I_L^{nom} will be used in the equations, which are calculated as follows:

$$I_L^{\mathrm{nom}} = \frac{V_s^{\mathrm{nom}}}{\sqrt{r_L^2 + (\omega L)^2}}. \tag{3}$$

A. Control of the Output Current i_L

In this case, it is necessary to generate an instantaneous current i_L with an effective value I_L and a phase angle ϕ, that corresponds to the angle between the grid voltage and the injected current i_L. If the effective value I_{L} and phase angle ϕ of the current are controlled, it will be possible to indirectly control the output power of the inverter. Since the grid is considered to be stiff, the effective value V_S of the grid voltage will be practically a constant and the power injected by the inverter can be written as:

$$P_o = V_S I_L \cos(\phi). \tag{4}$$

By a simple inspection of (4), it is possible to find that the injected power is maximum when the phase angle is zero (cos $(\phi) = 1$). Fig. 2(a) shows the plot of the power P_o as a function of the magnitude I_L and angle ϕ.

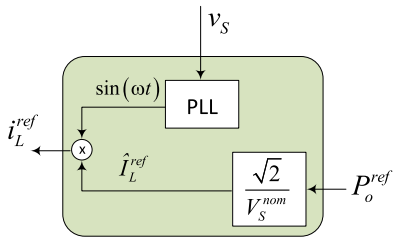

Fig. 3. Block diagram of the current reference generation subsystem.

By controlling the output current of the inverter, its output voltage V_{o} results in an uncontrolled variable that basically depends on the current imposed by the inverter, the grid voltage, and the line impedance in the following way:

$$V_o = \sqrt{\begin{array}{l}\left(I_L\sqrt{r_L^2+(\omega L)^2}\cos\left(\operatorname{atan}\left(\frac{\omega \mathrm{L}}{\mathrm{r_L}}\right)+\phi\right)+\mathrm{V_S}\right)^2 \\ +\left(I_L\sqrt{r_L^2+(\omega L)^2}\sin\left(\operatorname{atan}\left(\frac{\omega \mathrm{L}}{\mathrm{r_L}}\right)+\phi\right)\right)^2\end{array}} \tag{5}$$

where r_{L} and L are parameters of the ac line and ω is the grid angular frequency. If this voltage is plotted as a function of the effective value of current I_L and the phase angle ϕ [see Fig. 2(b)], it is possible to observe that for a nominal current value $I_L = I_L^{\mathrm{nom}}$, a nominal voltage of equal magnitude than the nominal voltage of the grid is obtained. In addition, it is possible to see that for the nominal current and a phase angle $\phi = \pi/2$, the output voltage in the inverter is zero. The latter allows defining a secure operation point with zero power injection and zero voltage, for a nominal current value in the system.

B. Generating a Sinusoidal Current Reference for a Desired Output Power

In order to control the output power by means of controlling the inverter output current i_L, a sinusoidal reference for the

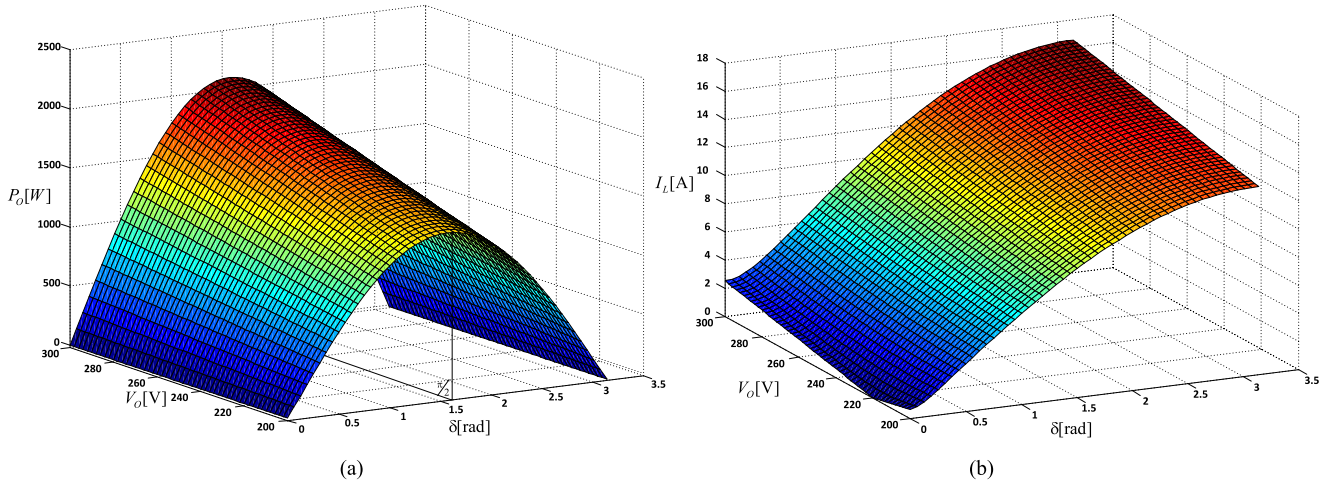

(a) (b)

Fig. 4. Output power and current of the SP-CSI as a function of the effective value V_o and power angle δ: (a) output power of the SP-CSI and (b) output current of the SP-CSI.

current has to be generated and a tracking control scheme has to be proposed. Given a desired output power, the reference current is defined by (4) with a phase angle ϕ equal to zero for a maximum power. Fig. 3 depicts the block diagram for the generation of the current reference.

As we can see from Fig. 3, the block in charge of producing the reference current must considerate a phase-lock loop that generates a synchronized signal in phase with the grid voltage. If proper synchronization is assumed, the amplitude of the desired current is just the division between the desired power and the nominal effective voltage of the grid.

C. Control of the Output Voltage v_o

If the inverter output power is indirectly controlled by managing the magnitude of the output voltage (V_o) and the phase angle δ with respect to the grid voltage (which is also known as power angle), it is possible to find that the power delivered to the grid is described by

$$P_o = V_S I_L \cos\left(\operatorname{atan}\left(\frac{V_o \sin(\delta)}{V_o \cos(\delta) - V_S}\right) - \operatorname{atan}\left(\frac{\omega L}{r_L}\right)\right). \tag{6}$$

In this case, the output current I_L is a noncontrolled variable and its value will be determined by the output voltage and the impedance of the ac line in the following way:

$$I_L = \sqrt{\frac{(V_o \cos(\delta) - V_S)^2 + (V_o \sin(\delta))^2}{r_L^2 + (\omega L)^2}}. \tag{7}$$

If the output power given in (6) is plotted against the output voltage imposed by the inverter and the power angle, it is possible to find that for any specific output voltage, the power injected by the inverter is maximum when the power angle δ is 90°, as shown in Fig. 4(a).

If the output current is plotted as a function of the effective output voltage imposed by the inverter and the power angle [see Fig. 4(b)], it can be noticed that for a nominal output voltage (equal to the grid voltage) and a power angle equal to zero, the output current I_{L} is zero. This allows defining a secure operation point with zero power injection.

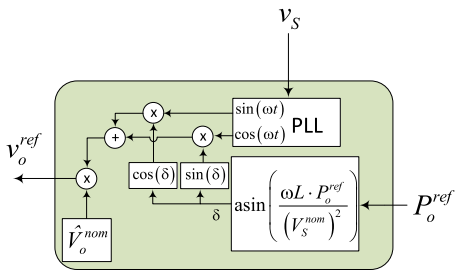

Fig. 5. Generation of the reference for the inverter output voltage.

D. Generating a Sinusoidal Voltage Reference for a Desired Output Power

If the output power is controlled by means of the output voltage of the inverter, now a voltage reference has to be generated. By neglecting the resistive part of the ac line, i.e., considering it as an inductive line, it is possible to simplify (6) and define the output active power as

$$P_o = \frac{V_S V_o}{\omega L} \sin(\delta). \tag{8}$$

From this equation, it can be noted that if the output voltage is kept at its nominal amplitude ($\hat{V}_o^{\mathrm{nom}}$), then it is possible to control the output power only by varying the power angle. However, because the value of the output inductance highly influences the calculation of the power reference, it is important to assure a good measurement of its value. Taken this into account, it is possible to propose a block that generates a reference voltage v_o^{ref} that depends on the value of the desired output power P_o^{ref} and on a synchronization signal with the grid voltage. This block is shown in Fig. 5.

It is worth to mention that the strategies for tracking a sinusoidal current or voltage can be applied to a single inverter or to a group of them connected in cascade. In the case of cascaded

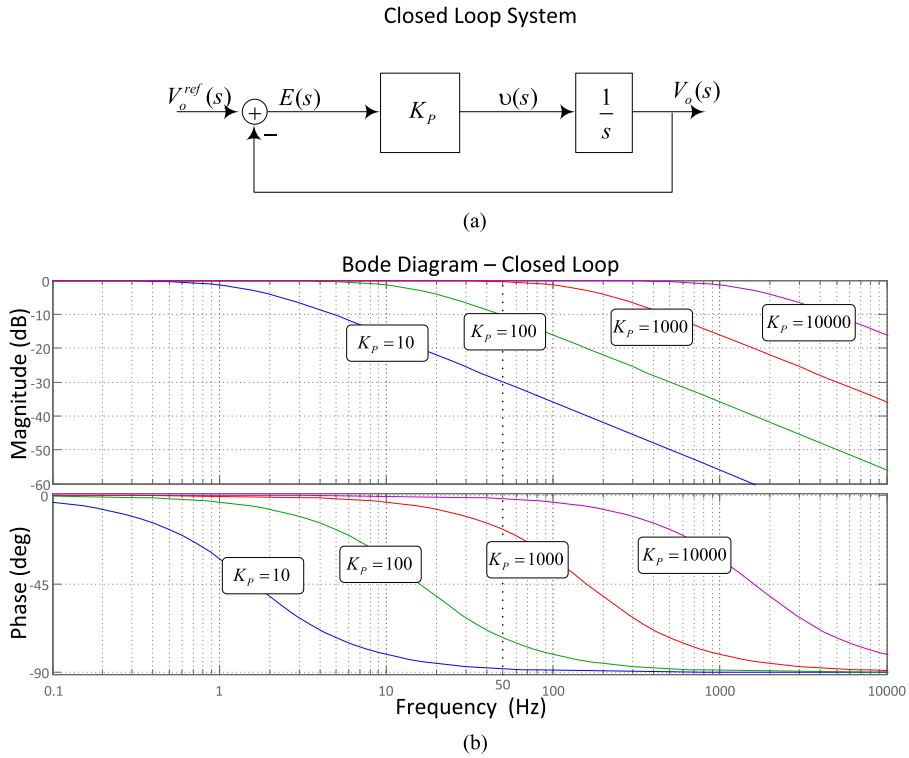

Fig. 6. Linearized system with P controller. (a) Block diagram of the control scheme, and (b) Bode plots for different values of K_p.

inverters [35], [36], the recommended strategy is to manage the output voltage on each inverter. By doing this, the total sharing of the total output voltage is assured and each inverter operates at a known safe voltage level [37]. Also, another application that requires controlling the output voltage—instead of the current—of an inverter connected to the grid is the virtual synchronous machine (VSM). A VSM is implemented with an inverter that injects power into the grid in such a way that it emulates the behavior of a synchronous machine; therefore, it can support the control of the grid frequency and voltage [35], [38]–[41]. For this reason, this paper focuses on a strategy to track sinusoidal voltage rather than current to control the output power of a grid-connected CSI.

IV. Proposals for Tracking Sinusoidal Voltage References in an SP-CSI

This paper presents an original method for tracking a sinusoidal voltage reference and it is based on a classical nonlinear control strategy called input–output linearization. Using the proposed strategy, two types of controllers will be evaluated in tracking a sinusoidal reference, a simple P controller and a PR controller.

A. Input–Output Linearization in the SP-CSI

Using the concept of average model for a pulse-width modulated (PWM) converter, it is possible to approximate a switching function $S_{\rm AC}$ to a sine function $m_{\rm AC}$ that represents the fundamental component of the switching function as follows:

$$\left.\begin{aligned} S_{\rm AC} &= M\sin(\omega t+\varphi)+\sum_{n=1}^{\infty} M_{n+1}\sin\left((n+1)\omega t+\varphi_{n+1}\right) \\ &\approx m_{\rm AC} = M\sin(\omega t+\varphi)). \end{aligned}\right\} \tag{9}$$

Thus, if we consider the fundamental component of the switching function $m_{\rm AC}$ as the input signal to the model given in (1), it will render the average model needed to apply the exact input–output linearization in the time domain. Considering (1) and (9), the output voltage of the inverter can be written as

$$\frac{dv_o}{dt} = \frac{1}{C_o}\left(m_{\rm AC} i_{\rm DC} - i_L\right). \tag{10}$$

Now, considering the output voltage as the system output

$$y = v_o \tag{11}$$

gives that the system's output derivative simply corresponds to (10)

$$\dot{y} = \frac{dv_o}{dt} = \frac{1}{C_o}\left(m_{\rm AC} i_{\rm DC} - i_L\right). \tag{12}$$

Then, from the procedure given in [42], it is possible to find the equations that make a system linear by successively differentiating the outputs of the system until finding the original inputs of the system in the resulting expressions. From (12), it can be seen that only one single differentiation with respect to time is needed for the system input $m_{\rm AC}$ to appear in the resultant mathematical expression.

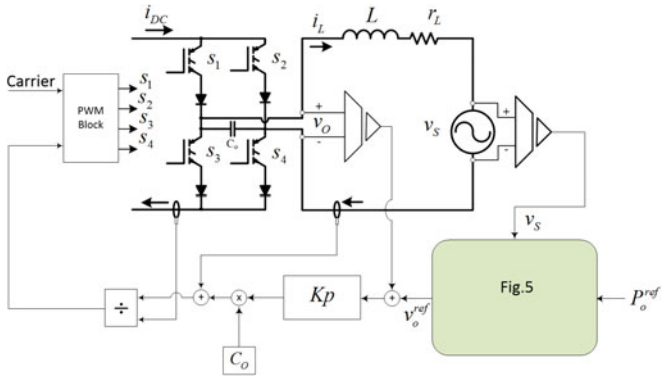

Fig. 7. Nonlinear control scheme of an SP-CSI using a P controller.

If a new input is conveniently defined as the derivative of the output as

$$\upsilon = \frac{1}{C_o}\left(m_{\mathrm{AC}} i_{\mathrm{DC}} - i_L\right) \tag{13}$$

we can easily find that the input that linearizes the system is

$$m_{\mathrm{AC}} = \frac{\upsilon C_o + i_L}{i_{\mathrm{DC}}} \tag{14}$$

with υ being the new input to the system. Now, the system (10) is linear with respect to the output v_o and the new input υ. By substituting (14) into (10), the result is the linearized system in the following form:

$$\frac{dv_o}{dt} = \upsilon. \tag{15}$$

B. Proportional Control of the Linearized SP-CSI

As can be seen from (15), the resulting system from the exact linearization is a pure integrator. From the classical control theory, in a system like this and where the input reference and the output variable is a dc quantity, the simplest controller capable of achieving zero error in steady state is the proportional one, i.e., a gain. However, when the reference is sinusoidal, if a P controller is used, it is only possible to achieve oscillating errors around zero, whose oscillation amplitude can be very small if the controller gain is very large. When using a gain as the controller of the linearized system, as shown in Fig. 6(a), one must ensure this gain K_p be as large as possible in order to increase the bandwidth in which the closed-loop gain is unitary with respect to the input. Moreover, the phase lag between the reference and the output voltage is closer to zero for a higher bandwidth, as shown in Fig. 6(c). Therefore, the higher the gain of the controller, the better the tracking of the reference voltage at the inverter output.

The proposed control strategy that integrates the above exact input–output linearization scheme and a P controller for the control of the output power of an SP-CSI connected to the grid is depicted in Fig. 7.

Despite its simplicity, proportional control has to overcome the problem of noise amplification. With a higher gain value K_P, the error between the reference and the output is amplified, effectively resulting in a better tracking, as we can predict by looking at the Bode plots in Fig. 6. However, this amplification produces at the same time an increased noise in the modulator, which induces a higher and variable switching frequency, increasing the switching losses in the converter. This means that in order to tune the proportional gain K_p, we must find a balance between switching frequency and tracking speed, which can only be done in a practical way. To improve the tracking of a sinusoidal reference and achieve zero error in steady state, without using high values of K_P and without increasing the switching frequency of the converter, a PR controller must be used [43].

C. PR Control of the Linearized SP-CSI

The strategies for tracking sinusoidal references based on PR control have been around for at least two decades [43], [44]. The main idea of a PR control is to emulate the infinite gain provided by a PI for a dc variable in open loop. This infinite gain of the PR allows eliminating the steady-state error in closed-loop for a specific frequency of design.

In Laplace domain, the resonant controller can be written as

$$C_{\mathrm{PR}}(s) = K_P + K_r \frac{s}{s^2 + \omega_0^2} \tag{16}$$

where K_P is the proportional gain and K_r is the resonant gain of the controller. The resonant part of the controller can be considered as a generalized integrator for ac variables, as it is mentioned in [45].

Fig. 8 shows the Bode plot of the average model of system (15) plus the *PR* controller (16) designed for 50 Hz, both in open- and closed-loop configurations. From the Bode plots, it can be seen that the controller introduces a very high gain in the open-loop system at the frequency of design [see Fig. 8(a)]. On the other hand, in the Bode diagram of the closed-loop system [see Fig. 8(b)], it is observed that the effect of the PR control system is to maintain a unity gain and zero phase lag for the resultant transfer function between the ac variables at 50 Hz. The latter indicates that the control in that frequency of resonance will perform a theoretical perfect tracking of the reference signal.

In order to implement the control strategy in a digital control card, the controller proposed in (16) has to be properly discretized. Using an impulse invariant method as the one proposed in [46], the controller (15) written in the discrete Z-domain has the following form:

$$C_{\mathrm{PR}}(z) = K_P + K_r T_S \frac{1 - z^{-1}\cos\left(\omega_0 T_S\right)}{1 - 2z^{-1}\cos\left(\omega_0 T_S\right) + z^{-2}}. \tag{17}$$

where ω_0 is the resonant frequency, T_S is the sampling period of the digital control, K_P is the proportional gain, and K_r is the resonant gain obtained at the resonant frequency ω_0. This control strategy is implemented as depicted in Fig. 9.

The tuning of the PR controller parameters is based on the approach proposed in [47].

V. Simulated Results of the Proposed Schemes

In order to test the design of the controllers and the theoretical premises of this paper, steady-state output voltage tracking and

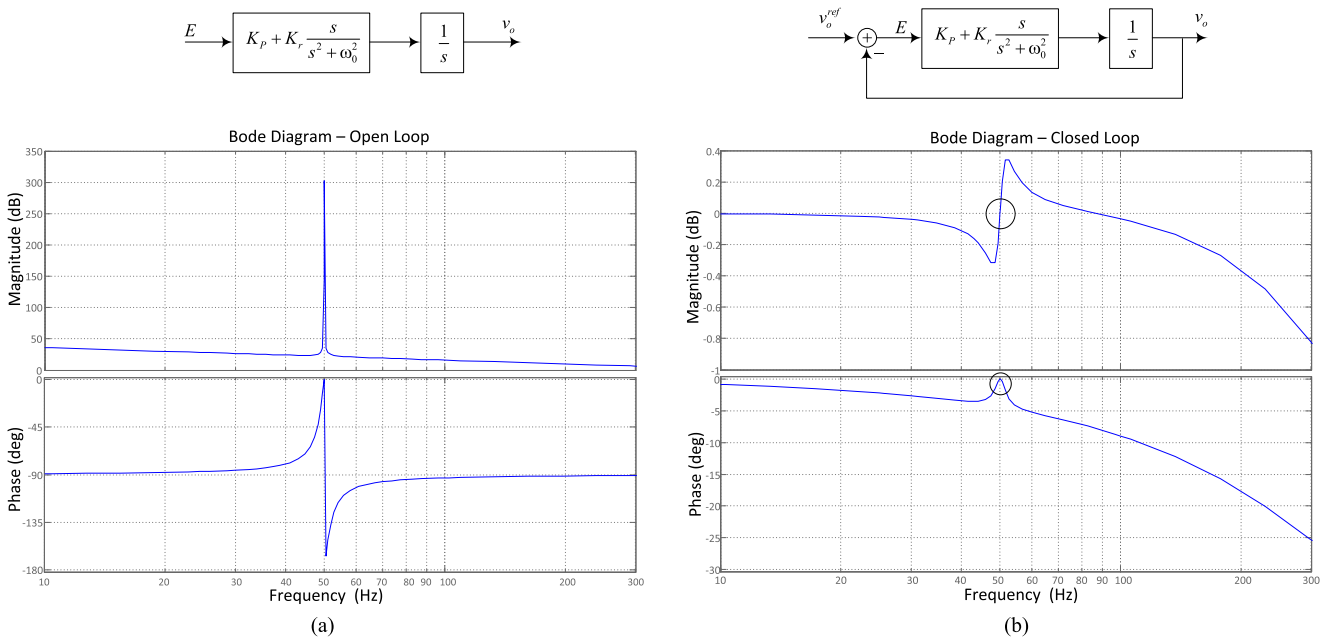

(a) (b)

Fig. 8. Block diagram and Bode plots of the linearized system with a PR controller. (a) Open-loop scheme, and (b) closed-loop scheme.

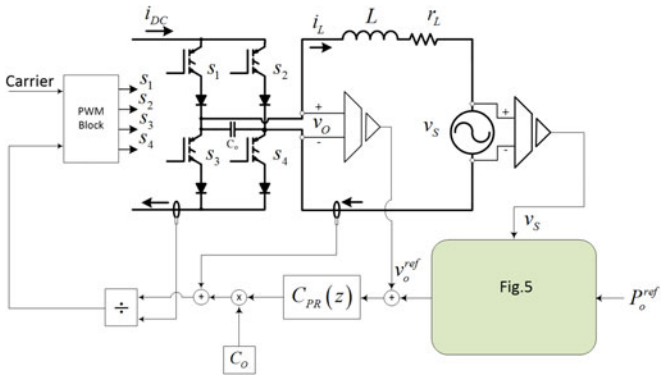

Fig. 9. Nonlinear control scheme for the SP-CSI using a PR controller.

TABLE I
PARAMETERS OF THE SYSTEM USED IN SIMULATIONS AND EXPERIMENTAL RESULTS

Parameters and/or Variables	Symbol	Value
Output capacitor	C_o	30 uF
Line inductance	L	86 mH
Line resistance	r_L	0.7 Ω
P. gain—for P control	K_P	3.1e3
P. gain—for PR control in S.S.	K_P	0.5e3
P. gain—for PR used for D.R	K_P	3.1e3
Resonant gain for PR control	K_r	1e5
Switching frequency	f_{sw}	550 Hz
Sampling period	T_s	100 μs
DC current	i_{DC}	2.4 A

Note: S.S.: Steady state and D.R: Dynamic response.

dynamic simulations for sudden changes in the power injected into a single-phase stiff grid will be performed. For all simulations, the parameters of the system are chosen to be the ones of the laboratory prototype. Parameters are summarized in Table I.

A. Behavior of the System in Steady State Using the Nonlinear Proportional Control Scheme

Simulations consider an SP-CSI connected to a stiff grid, where the inverter is modulated through a simple sinusoidal PWM technique with a carrier of 550 [Hz], with the purpose of achieving a low switching frequency.

Three simulations considering values of $K_P = 0.5\mathrm{e}3, 3.1\mathrm{e}3$, and $10\mathrm{e}3$ were performed. The results of these simulations for the waveforms of the reference and output voltages are shown in Fig. 10. Observing the behavior for the three different values of the proportional gain, the first conclusion is that for a higher gain there is a better tracking of the sinusoidal reference voltage, which was expected from the analysis of the Bode plot in Fig. 6. Furthermore, we can see that with a higher gain there is less total harmonic distortion (THD) in the output voltage waveform. The simulation also shows that when system operates with a higher gain in the controller, the power spectrum of the output voltage is not concentrated at multiples of the switching frequency, as we can see in Fig. 10(d) and (e), and it is rather distributed across the frequency range, as shown in Fig. 10(f). As discussed before, the latter condition must be avoided because it produces higher switching losses in the CSI. Therefore, it is not desirable to operate with high values for the proportional gain.

B. Behavior of the System in Steady State Using the Nonlinear PR Control Scheme

For this simulation, the parameters of the resonant controller are $K_P = 0.5\mathrm{e}3$ and $K_r = 1\mathrm{e}5$. The reference, the output voltage, and its associated power spectrum are shown in Fig. 11. In Fig. 11(a), it is possible to observe, practically a zero

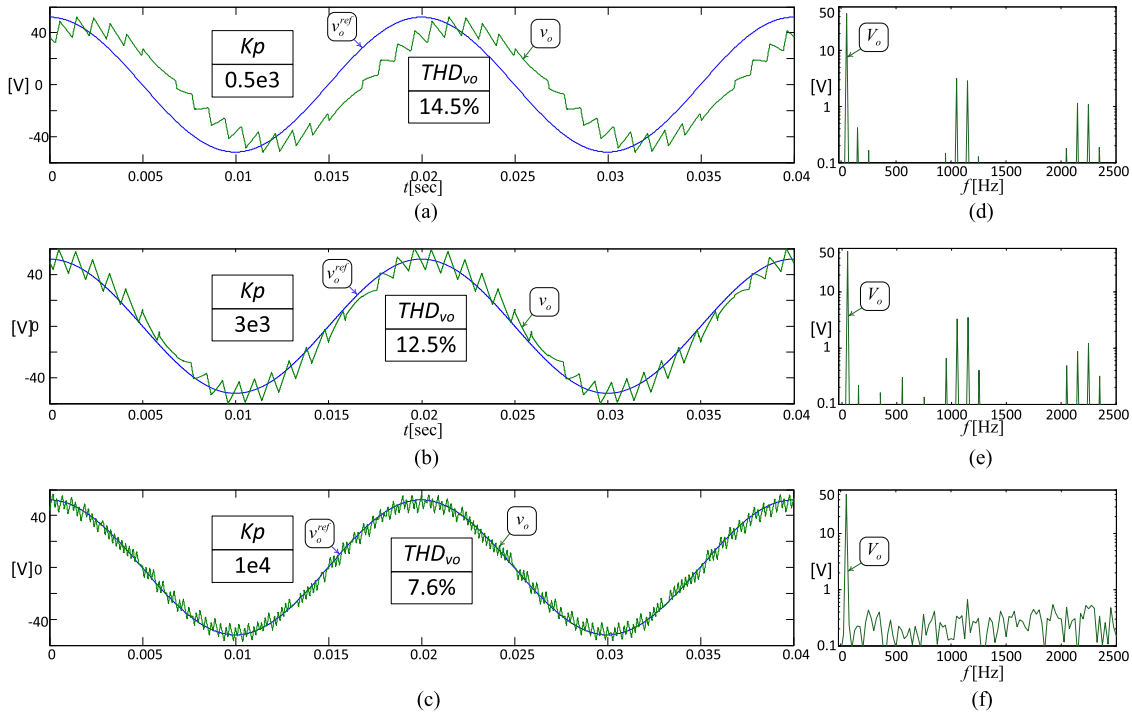

Fig. 10. Steady-state response of the P controller and associated frequency spectrum. Reference and inverter output voltage for different values of K_P: (a) $K_P = 0.5\text{e}3$, (b) $K_P = 3\text{e}3$, (c) $K_P = 1\text{e}4$; (d) spectrum of the output voltage in (a); (e) spectrum of the output voltage in (b); and (f) spectrum of the output voltage in (c).

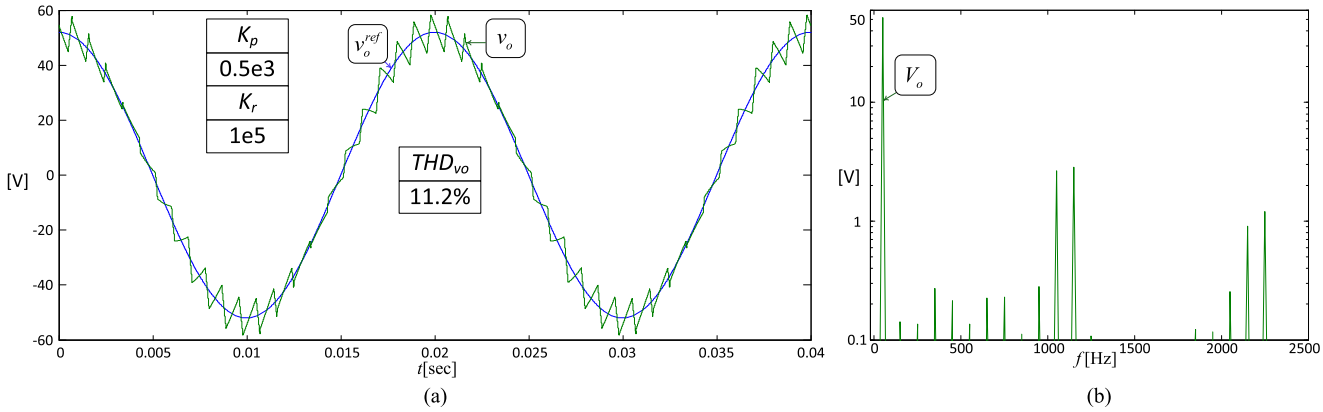

Fig. 11. Steady-state response of the PR controller and associated waveforms. (a) Reference and inverter output voltages, and (b) power spectrum of the output voltage.

steady-state error at fundamental frequency in the output voltage of the converter to the given reference trajectory in steady state, which radically differs from the case of only proportional control shown in Fig. 10(a), for the same value of gain $K_P = 0.5\text{e}3$.

It is also possible to note that, as in the case of lower gains for a simple P controller and because of the modulation technique used, the harmonics of the output voltage are mostly concentrated in the lower part of the spectrum at odd multiples of the carrier frequency. It is also important to mention that for the same proportional gain used in the P controller, a lower THD is achieved for the PR case (11.2% versus 12.5% in P case). This occurs because of the smaller error achieved by the PR strategy between the sinusoidal reference and the output voltage.

C. Dynamic Response of the P and PR Control Schemes

A relevant aspect of the sinusoidal tracking control schemes is the rapid response that can be achieved upon a change in the reference or a disturbance. In this section, the dynamic response of the P and PR controllers is evaluated upon an abrupt change in the output power of the inverter from 20% to 100%. Parameters used in both simulations are shown in Table I and simulation results for the P and PR controllers are shown in Figs. 12 and 13, respectively.

By observing Fig. 12(a), it is possible to see that the P controller performs well achieving a rapid response to a sudden change in the reference voltage due to a power increase from 20% to 100%. Likewise, in Fig. 13(a), it can be observed that

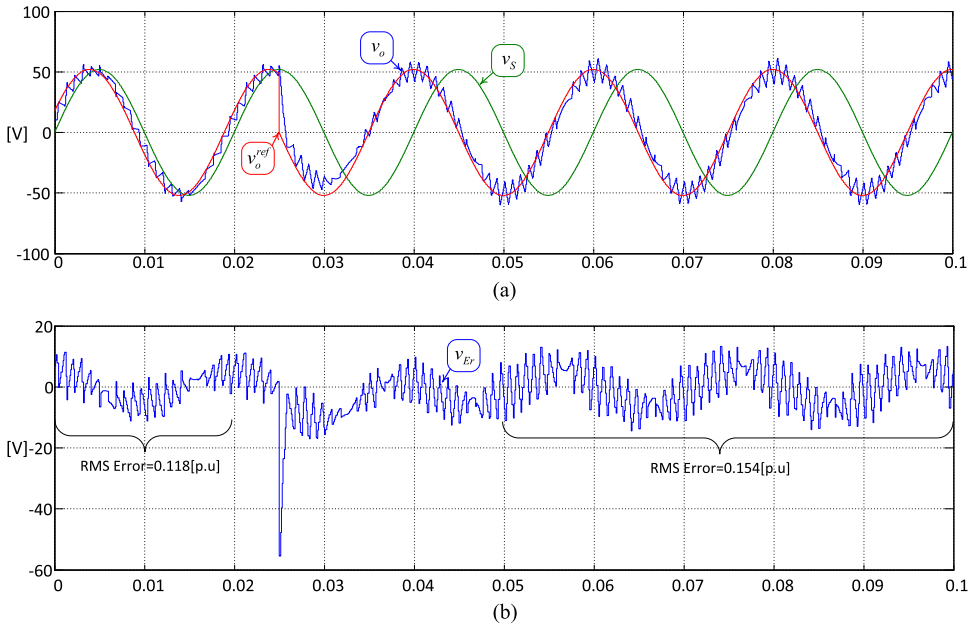

Fig. 12. Dynamic response of the P controller to a sudden increase in the output power. (a) Reference, inverter output, and grid voltage. (b) Control error between the reference and the output voltage of the SP-CSI.

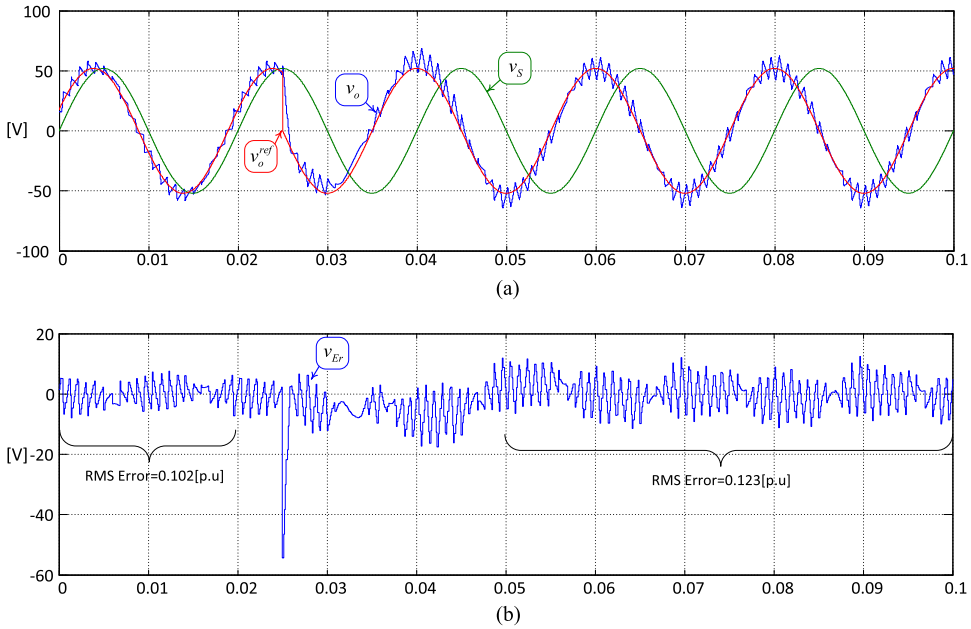

Fig. 13. Dynamic response of the PR controller to a sudden increase in the output power. (a) Reference, inverter output, and grid voltage. (b) Control error between the reference and the output voltage of the SP-CSI.

the inverter response with the PR controller achieves an even better response than the one of the P controller, since it is possible to notice that there is not an oscillating error around zero at fundamental frequency. To compare the tracking performance of both controllers the normalized root-mean-square measure of the control error (NRMSE) will be used. The NRMSE is defined as

$$\text{NRMSE} = \frac{\sqrt{\frac{1}{T}\int_0^T \left(v_o^{\text{ref}}(t) - v_o(t)\right)^2 dt}}{V_{o(\text{rms})}^{\text{ref}}} \qquad (18)$$

TABLE II
CONTROL ERROR IN P.U.

Index	Control Type	20% of Power in S.S.	100% of Power in S.S.	Transient State
NRMSE	P (see Fig. 12)	0.118 [p.u]	0.154 [p.u]	–
NRMSE	PR (see Fig. 13)	0.102 [p.u]	0.123 [p.u]	–
I_E	P (see Fig. 12)	–	–	0.678 [p.u]
I_E	PR (see Fig. 13)	–	–	0.564 [p.u]

Note: S.S.: Steady state.

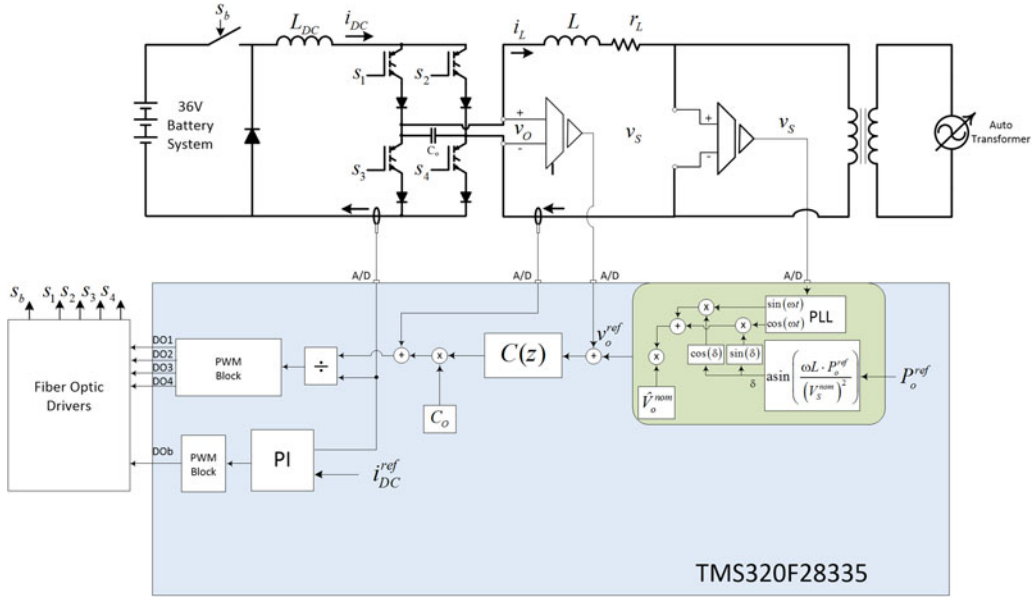

Fig. 14. Scheme of the experimental setup implemented at the laboratory.

where $V_{o(\mathrm{rms})}^{\mathrm{ref}}$ is the root-mean-square value of the reference in steady state. In addition, to compare both transient state errors, shown in Figs. 12(b) and 13(b), the following index based on the integral of the control error (I_E) within the transient period T_{T} is proposed:

$$I_E = \left| \frac{\int_0^{T_T} (v_o^{\mathrm{ref}}(t) - v_o(t))dt}{\int_0^{T_T} v_o^{\mathrm{ref}}(t)dt} \right|. \tag{19}$$

Table II summarizes the tracking error calculated in both simulations presented in Figs. 12 and 13. The calculation considers steady-state regime in low and maximum power for the NRMSE (18), and the error in the transient state given by index I_{E} (19).

Looking at the results in Table II, it can be noted that the lowest errors are achieved by using the PR tracking scheme. Nevertheless, the P controller can still be considered a plausible control strategy to be used in preliminary testing stages where there is no guarantee of a good performance of the PR, e.g., when the converter is tested operating at different values of grid frequency.

VI. Experimental Results

In order to validate the theoretical premises of this paper and the simulated results, a laboratory prototype is built to conduct experimental tests. Parameters and variables of the implementation are summarized in Table I. The parameters of this prototype are the same to those used in simulations (see Table I). It is worth to mention that the inductor used in the ac side (86 mH) has not been optimized for the power level of the prototype and, therefore, this can be a source of considerable losses. For higher power levels, the size of the inductor must be carefully designed in order to keep the losses low. The dc bus of the converter is supplied by a small battery bank and a buck converter is responsible for ensuring a current of 2.4 [A] at the inverter input. A PI controller, necessary for the control of the dc current with the buck converter, and the proposed controller C(z)—which can be P or PR—responsible for the tracking of the output voltage of the inverter, are programmed into a DSP-TMS320F28335 Texas Instrument card. Fig. 14 presents a diagram of the experimental implementation.

A. Performance of the P Controller in Steady State

This section presents the evaluation of three practical experiences with the inverter injecting maximum power—90° in the power angle—into the single-phase grid. Three different values of K_P are used (0.5e3, 3.1e3, and 10e3) and the performance of the controller is evaluated in steady state. Fig. 15 shows the waveforms obtained in each case. As it was observed in simulations, the prototype exhibits poor tracking of the reference voltage as the proportional gain is low; however, on the contrary, the power spectrum improves. From the cases shown in Fig. 15, $K_P = 3\mathrm{e}3$ is of more interest because the controller shows acceptable tracking capability [see Fig. 15(b)] and the power spectrum is still representative of the carrier frequency being used [see Fig. 15(e)], which ensures that the commutation losses are not being increased excessively.

B. Performance of the PR Controller in Steady State

To avoid using large gains in the simple proportional control, a PR controller was proposed and experimentally evaluated. In Fig. 16(a), it can be observed that with a proportional gain $K_P = 0.5\mathrm{e}3$ and a resonant gain $K_r = 1\mathrm{e}5$ a more accurate tracking is achieved without increasing the harmonic content in the output voltage as it occurs in the cases with large proportional gains [see Fig. 16(b)]. In point of fact, if one compare Fig. 16(a) with Fig. 15(a) and (b), it is not so difficult to realize that this new proposal presents an output voltage amplitude closer to the sinusoidal reference amplitude.

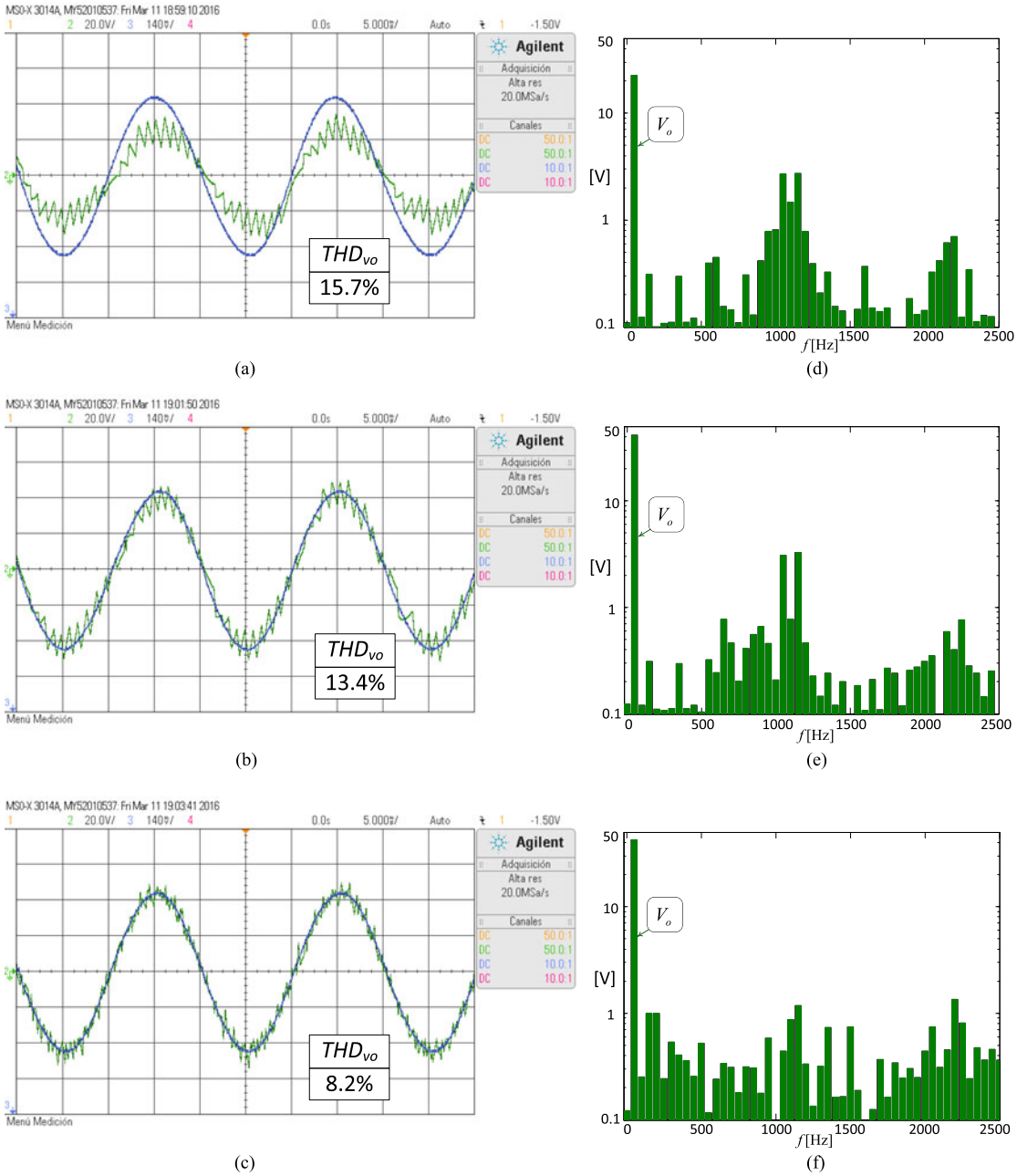

Fig. 15. Steady-state response of the P controller in experimental test and associated frequency spectrum. Reference and inverter output voltage for different values of K_P: (a) $K_P = 0.5\text{e}3$, (b) $K_P = 3\text{e}3$, (c) $K_P = 1\text{e}4$, (d) spectrum of the output voltage in (a). (e) Spectrum of the output voltage in (b), and (f) spectrum of the output voltage in (c).

As shown previously in simulations, it is possible to observe that for equal gains in both strategies (P and PR), a lower THD for the output voltage is obtained with the PR controller (11.8% versus 15.7% in P case). This can be explained by the better tracking capability of the PR controller.

C. Performance of the P and PR Controllers in Transient State

In order to analyze the transient response of both controllers, two practical experiments were performed, consisting in a sudden increase in the power delivered by the inverter to the grid from 20% to 100%. The summary of the parameters from both experiences is presented in Table I.

The results are presented in Fig. 17, where Fig. 17(a) shows the reference, the inverter output, and the grid voltages. The reference voltage is suddenly changed at time $t = 22$ ms, increasing the power angle from 15° to 90° almost instantly, forcing the output voltage to track the reference and change the power injected with a transient response of less than one grid cycle. Fig. 17(b) shows the control error between the reference signal and the output voltage, from which it is possible to calculate the performance indexes previously introduced: the integral of the error I_E for the transient regime and the NRMSE for the steady state before and after the transient, these data are presented in Table III.

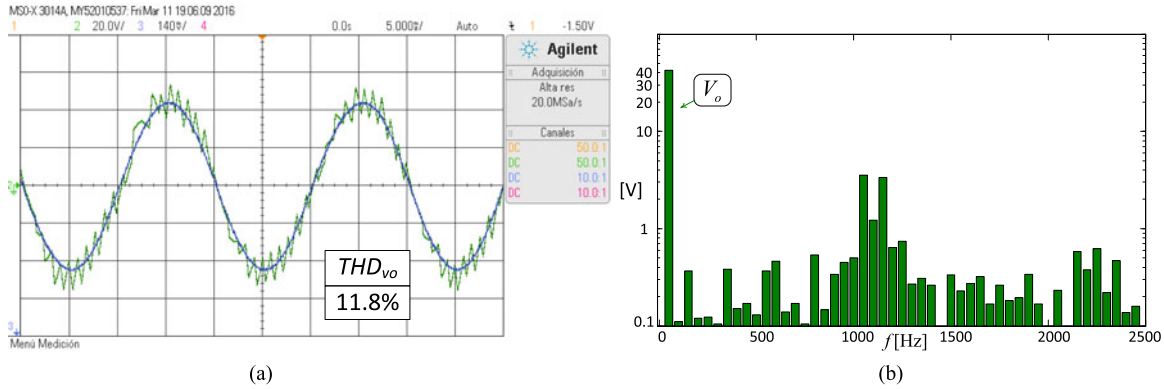

Fig. 16. Reference, inverter output voltage and its spectrum of the SP-CSI connected to a grid.

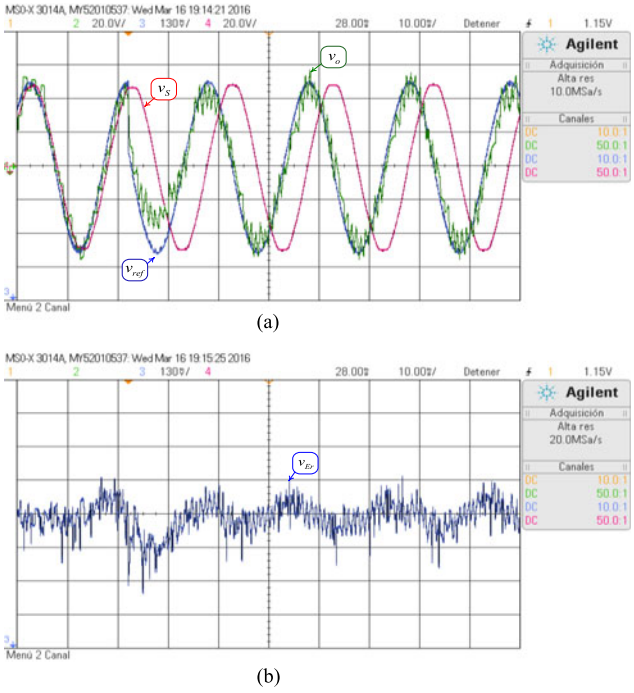

Fig. 17. Dynamic response in experimental test of the P controller to a sudden increase in the output power. (a) Reference, inverter output, and grid voltage. (b) Control error between the reference and the output voltage of the SP-CSI.

TABLE III
CONTROL ERROR IN P.U. FOR EXPERIMENTAL TESTS

Index	Control Type	20% of Power in S.S.	100% of Power in S.S.	Transient State
NRMSE	P (see Fig. 17)	0.121 [p.u]	0.164 [p.u]	–
NRMSE	PR (see Fig. 18)	0.092 [p.u]	0.133 [p.u]	–
I_E	P (see Fig. 17)	–	–	0.71 [p.u]
I_E	PR (see Fig. 18)	–	–	0.567 [p.u]

Note: S.S.: Steady state.

On the other hand, the waveforms of the dynamic response associated to the PR controller are presented in Fig. 18(a), where the reference, the output, and the grid voltage are shown. Again, the reference is changed at $t = 22$ ms, forcing the inverter to inject the 100% of the available power. The error between the reference and the output voltage of the inverter is shown in Fig. 18(b).

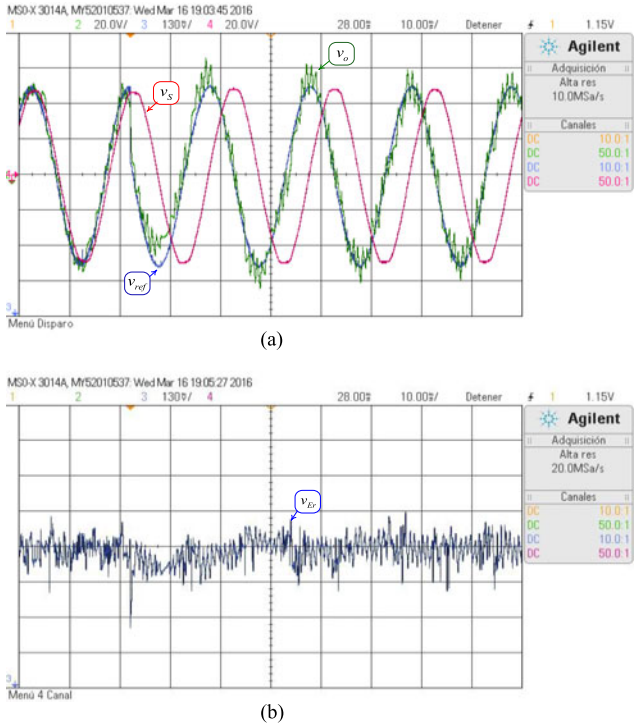

Fig. 18. Dynamic response in experimental test of the PR controller to a sudden increase in the output power. (a) Reference, inverter output, and grid voltage. (b) Control error between the reference and the output voltage of the SP-CSI.

The performance indexes I_E and NRMSE that allow evaluating the tracking error have also been calculated and are presented in Table III.

Waveforms presented in Figs. 17 and 18 and the experimental data of Table III demonstrate that the proposed control scheme achieves good tracking of the sinusoidal reference and, simultaneously, it allows low switching frequencies. An advantage of the scheme with PR controller over the P controller is that it achieves zero average error in steady state.

VII. CONCLUSION

This paper deals with sinusoidal reference tracking strategies for SP-CSIs connected to an ac grid. A novel control strategy for maximum power injection that entails the exact linearization of the inverter model was proposed, analyzed, and validated

experimentally. From the analysis of the Bode plots of the linearized system, it was determined that the output voltage of the inverter can be controlled simply by using a P controller, and also with a PR controller to achieve better dynamic performance. The simulated and experimental results demonstrate that both controllers can achieve a good tracking of the sinusoidal reference while keeping the switching frequency low, which helps to minimize the switching losses. The PR controller was found to be the best option, achieving the lowest tracking error, both in the steady state and transient regime. On the other hand, for the P controller, it was found that higher gains can improve the tracking, however, it also makes the switching harmonics to increase and become variable, affecting number of commutations per cycle and therefore the switching losses. Therefore, when tuning the P controller, it is recommended to look for a value of proportional gain that minimizes the error, but it does not introduce uncharacteristic harmonics in the voltage spectrum.

REFERENCES

[1] L. G. Franquelo, J. Rodriguez, J. I. Leon, S. Kouro, R. Portillo, and M. A. M. Prats, "The age of multilevel converters arrives," *IEEE Ind. Electron. Mag.*, vol. 2, no. 2, pp. 28–39, Jun. 2008.

[2] D. Barater, E. Lorenzani, C. Concari, G. Franceschini, and G. Buticchi, "Recent advances in single-phase transformerless photovoltaic inverters," *IET Renewable Power Gener.*, vol. 10, no. 2, pp. 260–273, 2016.

[3] G. Oriti, A. L. Julian, and N. J. Peck, "Power-electronics-based energy management system with storage," *IEEE Trans. Power Electron.*, vol. 31, no. 1, pp. 452–460, Jan. 2016.

[4] M. N. Arafat, S. Palle, Y. Sozer, and I. Husain, "Transition control strategy between standalone and grid-connected operations of voltage-source inverters," *IEEE Trans. Ind. Appl.*, vol. 48, no. 5, pp. 1516–1525, Sep./Oct. 2012.

[5] H. Tao, J. L. Duarte, and M. A. M. Hendrix, "Line-interactive UPS using a fuel cell as the primary source," *IEEE Trans. Ind. Electron.*, vol. 55, no. 8, pp. 3012–3021, Aug. 2008.

[6] L. Barote, C. Marinescu, and M. N. Cirstea, "Control structure for single-phase stand-alone wind-based energy sources," *IEEE Trans. Ind. Electron.*, vol. 60, no. 2, pp. 764–772, Feb. 2013.

[7] D. Sun, B. Ge, W. Liang, H. Abu-Rub, F. Z. Peng, "An energy stored quasi-Z-source cascade multilevel inverter-based photovoltaic power generation system," *IEEE Trans. Ind. Electron.* vol. 62, no. 9, pp. 5458–5467, Sep. 2015.

[8] B. Ge *et al.*, "Current ripple damping control to minimize impedance network for single-phase quasi-Z source inverter system," *IEEE Trans. Ind. Informat.*, vol. 12, no. 3, pp. 1043–1054, Jun. 2016.

[9] Y. Liu, B. Ge, H. Abu-Rub, and D. Sun, "Comprehensive modeling of single-phase quasi-Z-source photovoltaic inverter to investigate low-frequency voltage and current ripple," *IEEE Trans. Ind. Electron.*, vol. 62, no. 7, pp. 4194–4202, Jul. 2015.

[10] C. S. Thelukuntla and M. Veerachary, "Resonant controller based single-phase Z-source inverter with LCL-filter," in *Proc. Joint Int. Conf. Power Electron., Drives Energy Syst./2010 Power India*, New Delhi, India, 2010, pp. 1–6.

[11] B. N. Alajmi, K. H. Ahmed, G. P. Adam, and B. W. Williams, "Single-phase single-stage transformer less grid-connected PV system," *IEEE Trans. Power Electron.*, vol. 28, no. 6, pp. 2664–2676, Jun. 2013.

[12] R. T. H. Li, H. S. H. Chung, W. H. Lau, and B. Zhou, "Use of hybrid PWM and passive resonant snubber for a grid-connected CSI," *IEEE Trans. Power Electron.*, vol. 25, no. 2, pp. 298–309, Feb. 2010.

[13] P. E. Melin *et al.*, "Analysis and design of a multicell topology based on three-phase/single-phase current-source cells," *IEEE Trans. Power Electron.*, vol. 31, no. 9, pp. 6122–6133, Sep. 2016.

[14] C. R. Baier, M. Torres, J. A. Muñoz, R. A. Marco, E. N. Eduardo, and P. Acuña, "Bidirectional power flow control of a single-phase current-source grid-tie battery energy storage system," in *Proc. IEEE 24th Int. Symp. Ind. Electron.*, Buzios, Brazil, 2015, pp. 1372–1377.

[15] R. T. H. Li, H. S. H. Chung, and T. K. M. Chan, "An active modulation technique for single-phase grid-connected CSI," *IEEE Trans. Power Electron.*, vol. 22, no. 4, pp. 1373–1382, Jul. 2007.

[16] S. Jayalath and M. Hanif, "Controller tuning for a single phase grid-connected current source inverter," *Proc. IEEE 2nd Int. Future Energy Electron. Conf.*, Taipei, Taiwan, 2015, pp. 1–6.

[17] B. Sahan, S. V. Araújo, C. Nöding, and P. Zacharias, "Comparative evaluation of three-phase current source inverters for grid interfacing of distributed and renewable energy systems," *IEEE Trans. Power Electron.*, vol. 26, no. 8, pp. 2304–2318, Aug. 2011.

[18] S. A. Azmi, K. H. Ahmed, S. J. Finney, and B. W. Williams, "Comparative analysis between voltage and current source inverters in grid-connected application," in *Proc. IET Conf. Renewable Power Gener.*, Sep. 6–8, 2011, pp. 1–6.

[19] S. Catellani, A. Bier, J. Martin, L. Gabriel, and F. Barruel, "Characterization of 1.2kV silicon carbide (SiC) semiconductors in hard switching mode for three-phase current source inverter (CSI) prototyping," in *Proc. PCIM Eur. 2015; Int. Exhib. Conf. Power Electron., Intell. Motion, Renewable Energy Energy Manage.*, Nuremberg, Germany, 2015, pp. 1–8.

[20] R. Mitova, R. Ghosh, U. Mhaskar, D. Klikic, M. X. Wang, and A. Dentella, "Investigations of 600-V GaN HEMT and GaN diode for power converter applications," *IEEE Trans. Power Electron.*, vol. 29, no. 5, pp. 2441–2452, May 2014.

[21] H. Ma, X. Chen, and F. Xu, "Observer-based discrete-time sliding-mode control for single-phase current-source inverter," in *Proc. 37th Annu. Conf. IEEE Ind. Electron. Soc.*, Melbourne, VIC, Australia, 2011, pp. 1492–1496.

[22] B. Exposto, R. Rodrigues, J. G. Pinto, V. Monteiro, D. Pedrosa, and J. L. Afonso, "Predictive control of a current-source inverter for solar photovoltaic grid interface," in *Proc. 9th Int. Conf. Compat. Power Electron.*, Costa da Caparica, Portugal, 2015, pp. 113–118.

[23] Z. Wang, S. Fan, Z. Zou, Y. Huang, and M. Cheng, "Control strategies of current-source inverters for distributed generation under unbalanced grid conditions," in *Proc. IEEE Energy Convers. Congr. Expo.*, Raleigh, NC, USA, 2012, pp. 4671–4675.

[24] X. Hao, X. Yang, T. Liu, L. Huang, and W. Chen, "A sliding-mode controller with multiresonant sliding surface for single-phase grid-connected VSI with an LCL filter," *IEEE Trans. Power Electron.*, vol. 28, no. 5, pp. 2259–2268, May 2013.

[25] H. Gao, B. Wu, D. Xu, R. Aguilera, and P. Acuna, "Model predictive switching pattern control for current source converters with space-vector-based selective harmonic elimination," *IEEE Trans. Power Electron.*, vol. PP, no. 99, pp. 1–1, to be published.

[26] Y. W. Li, M. Pande, N. R. Zargari, and B. Wu, "DC-Link current minimization for high-power current-source motor drives," *IEEE Trans. Power Electron.*, vol. 24, no. 1, pp. 232–240, Jan. 2009.

[27] P. Mao, M. Zhang, W. Zhang, and B.-H. Kwon, "A review of current control strategy for single-phase grid-connected inverters" *TELKOMNIKA*, vol. 12, no. 3, pp. 563–580, Sep. 2014.

[28] I. Sefa, N. Altin, S. Ozdemir, and O. Kaplan, "Fuzzy PI controlled inverter for grid interactive renewable energy systems," *IET Renewable Power Gener.*, vol. 9, no. 7, pp. 729–738, 2015.

[29] J. Hu, J. Zhu, and D. G. Dorrell, "Model predictive control of grid-connected inverters for PV systems with flexible power regulation and switching frequency reduction," *IEEE Trans. Ind. Appl.*, vol. 51, no. 1, pp. 587–594, Jan./Feb. 2015.

[30] Q. Wang, M. Cheng, and Y. Jiang, "Harmonics suppression for critical loads using electric springs with current-source inverters," *IEEE J. Emerg. Sel. Topics Power Electron.*, vol. 4, no. 4, pp. 1362–1369, Dec. 2016.

[31] P. Cossutta, M. P. Aguirre, A. Cao, S. Raffo, and M. I. Valla, "Single-stage fuel cell to grid interface with multilevel current-source inverters," *IEEE Trans. Ind. Electron.*, vol. 62, no. 8, pp. 5256–5264, Aug. 2015.

[32] H. Gao, B. Wu, D. Xu, M. Pande, and R. Aguilera, "Common-mode voltage reduced model predictive control scheme for current source converter-fed induction motor drives," *IEEE Trans. Power Electron.*, vol. 32, no. 6, pp. 4891–4904, Jun. 2017.

[33] J. Rohten *et al.*, "Resonant control for multi-cell cascaded H-bridge topologies based on current source inverters," in *Proc. 40th Annu. Conf. IEEE Ind. Electron. Soc.*, Dallas, TX, USA, 2014, pp. 1754–1759.

[34] M. Torres, C. Baier, J. Silva, and J. Espinoza, "On the control of a grid-connected photovoltaic plant under non-uniform insolation," in *Proc. 40th Annu. Conf. IEEE Ind. Electron. Soc.*, Dallas, TX, USA, 2014, pp. 5565–5570.

[35] P. E. Melín, J. R. Espinoza, J. A. Rohten, E. E. Espinosa, C. R. Baier, and J. I. Guzman, "Cascaded H-bridge topologies comparison for multi-cell current-source inverters under different DC inductor size reduction methods," in *Proc. 40th Annu. Conf. IEEE Ind. Electron. Soc.*, Dallas, TX, USA, 2014, pp. 4568–4574.

[36] C. R. Baier, M. Torres, J. A. Muñoz, J. M. Mauricio, J. Rohten, and M. Rivera, "Nonlinear control strategy for current source cascaded H-bridge inverters—An approach considering single-phase DQ components," in *Proc. Int. Conf. Ind. Technol.*, Seville, Spain, 2015, pp. 3079–3084.
[37] C. R. Baier *et al.*, "d-q-DC reference frame control strategy for single-phase current source cascaded inverters," in *Proc. 40th Annu. Conf. IEEE Ind. Electron. Soc.*, Dallas, TX, USA, 2014, pp. 4615–4621.
[38] J. M. Guerrero, M. Chandorkar, T. Lee, and P. C. Loh, "Advanced control architectures for intelligent microgrids-Part I: Decentralized and hierarchical control," *IEEE Trans. Ind. Electron.*, vol. 60, no. 4, pp. 1254–1262, Apr. 2013.
[39] Y. Li and Y. W. Li, "Power management of inverter interfaced autonomous microgrid based on virtual frequency-voltage frame," *IEEE Trans. Smart Grid*, vol. 2, no. 1, pp. 30–40, Mar. 2011.
[40] M. Torres and C. Baier, "Design of a virtual synchronous generator strategy for a single-phase current-source inverter," in *Proc. IEEE 24th Int. Symp. Ind. Electron.*, Buzios, Brazil, 2015, pp. 482–487.
[41] T. Shintai, Y. Miura, and T. Ise, "Oscillation damping of a distributed generator using a virtual synchronous generator," *IEEE Trans. Power Del.*, vol. 29, no. 2, pp. 668–676, Apr. 2014.
[42] J. Zhou and X. Lu, "Review of exact linearization method applied to power electronics system," in *Proc. 2012 Asia-Pac. Power Energy Eng. Conf.*, Shanghai, China, 2012, pp. 1–4.
[43] Y. Sato, T. Ishizuka, K. Nezu, and T. Kataoka, "A new control strategy for voltage type PWM rectifiers to realise zero steady-state control error in input current," in *Conf. Rec. 1997 IEEE Ind. Appl. Conf., 32th IAS Annu. Meeting*, New Orleans, LA, USA, 1997, pp. 1496–1503, vol. 2.
[44] Y. Sato, T. Ishizuka, K. Nezu, and T. Kataoka, "A new control strategy for voltage-type PWM rectifiers to realize zero steady-state control error in input current," *IEEE Trans. Ind. Appl.*, vol. 34, no. 3, pp. 480–486, May/Jun. 1998.
[45] R. Teodorescu, F. Blaabjerg, M. Liserre, and P. C. Loh, "Proportional-resonant controllers and filters for grid-connected voltage-source converters," *IEE Proc. Elect. Power Appl.*, vol. 153, no. 5, pp. 750–762, Sep. 2006.
[46] A. G. Yepes, F. D. Freijedo, J. Doval-Gandoy, O. López, J. Malvar, and P. Fernandez-Comesaña, "Effects of discretization methods on the performance of resonant controllers" *IEEE Trans. Power Electron.*, vol. 25, no. 7, pp. 1692–1712, Jul. 2010.
[47] A. Vidal *et al.*, "Assessment and optimization of the transient response of proportional-resonant current controllers for distributed power generation systems," *IEEE Trans. Ind. Electron.*, vol. 60, no. 4, pp. 1367–1383, Apr. 2013.

Carlos R. Baier (S'08–M'11) was born in Temuco, Chile, in 1979. He received the B.S., M.Sc., and D.Sc. degrees in electrical engineering from the University of Concepcion, Concepcion, Chile, in 2004, 2006, and 2010, respectively.

Since 2009, he has been a Professor in the Faculty of Engineering, Universidad de Talca, Talca, Chile, where he is teaching in the areas of industrial electronics. His research interests include improved control techniques for multicell converters, new multilevel topologies to inject power into the grid, and high energy efficient improvements for medium-voltage converters.

Miguel A. Torres (S'08–M'13) received the Graduate degree in electronics engineering and the M.Sc. degree in electrical engineering from Universidad de Concepción, Concepción, Chile, in 2004 and 2007, respectively, and the Ph.D. degree in electrical engineering from Concordia University, Montreal, QC, Canada, in 2013.

In 2003, he was with the L'École Supérieure d'Électricité (SUPÉLEC), Paris, France, working on passivity-based control of voltage-source converters. From 2005 to 2008, he worked in the industry as an Automation Engineer. From 2013 to 2016, he was with the Chilean Solar Energy Research Center, Department of Electrical Engineering, University of Concepción, as a Postdoctoral Fellow, where he is currently working on the control of multicell converter topologies for the integration of large-scale photovoltaic plants into the grid. He is currently with the Institute of Engineering Sciences, Universidad de O'Higgins, Rancagua, Chile.

Pablo Acuna (M'12) received the B.Sc. degree in electronics engineering, the Electronics Engineering Professional degree, and the Ph.D. degree in electrical engineering from the University of Concepcion, Concepcion, Chile, in 2004, 2007, and 2013, respectively.

He is currently a Research Associate at the University of New South Wales, Sydney, NSW, Australia. His research interests include electrical power conversion systems and their applications to industry, transportation, and utility.

Javier A. Muñoz (S'08–M'12) received the Eng. degree in electronic engineering (with First Class Hons.) and the M.Sc. and D.Sc. degrees in electrical engineering from the University of Concepción, Concepción, Chile, in 2007, 2009, and 2012, respectively.

Since April 2011, he has been with University of Talca, Curicó, Chile, where he recently joined the Department of Electrical Engineering. He is currently teaching in the areas of dynamic systems and robotics and his research interests include asymmetric converters to photovoltaic integration to microgrids.

Pedro E. Melín (S'10–M'14) was born in Chillán, Chile, in 1982. He received the Eng. degree in electronic engineering, and the M.Sc. and D.Sc. degrees in electrical engineering from the University of Concepción, Concepción, Chile, in 2006, 2010, and 2014, respectively.

Since 2013, he has been with the Department of Electrical and Electronic Engineering, University of Bío-Bío, Concepción, Chile, where he is currently an Assistant Professor, teaching in the areas of electronic applications and digital systems. His research interest include voltage-source and current-source converters and their extension to multilevel topologies, including their design, digital control and the application of this kind of topologies to ac drives, active power filters, and energy conversion.

Carlos Restrepo received the Bachelor's degree (Hons.) and the Master's degree in electrical engineering in 2006 and 2007, respectively, from the Universidad Tecnológica de Pereira, Pereira, Colombia, and the Master degree and the Ph.D. (Hons.) degree in electronic engineering from the Universitat Rovira i Virgili de Tarragona, Tarragona, Spain, in 2008 and 2012, respectively.

He was a Visiting Scholar with the Faculty of Electrical Engineering and Computer Science, University of Maribor, Slovenia, in 2011. During 2013 and 2014, he was a Postdoctoral Researcher with the Electrical Power Processing Group, Delft University of Technology, Delft, The Netherlands. From 2014 to 2016, he was a Professor with the Departamento de Ingeniería Eléctrica, Universidad Técnica Federico Santa María, Santiago de Chile, Chile. He is currently a Professor with the Departamento de Ingeniería Eléctrica, Universidad de Talca, Curicó, Chile. His main research interests include modeling and emulator design for fuel cells, design and digital control of switched converters, and offshore wind farm integration into the power systems.

Johan I. Guzman (S'04–M'09) was born in Chile in 1976. He received the Electronic Engineering title, and the M.Sc. and D.Sc. degrees in electrical engineering from the University of Concepcion, Concepción, Chile, in 2000, 2007, and 2009, respectively.

Since 2006 to 2008 he was lecturer at the University of Concepcion and the University of Desarrollo. Currently he is at the University of Talca, Curicó, Chile, where he has been since 2008, holding the position of assistant professor since 2010. He has consulting experience on energetic efficiency and integration of new technologies for little and medium business. His active research topics are power converters control for magnetic coupled converters and use of ERNC in isolated communities.